



Metastable Polymeric Nitrogen: The Ultimate Green High-Energy-Density Material

by Jennifer A. Ciezak

ARL-TR-4478

June 2008

NOTICES

Disclaimers

The findings in this report are not to be construed as an official Department of the Army position unless so designated by other authorized documents.

Citation of manufacturer's or trade names does not constitute an official endorsement or approval of the use thereof.

Destroy this report when it is no longer needed. Do not return it to the originator.

Army Research Laboratory

Aberdeen Proving Ground, MD 21005-5066

ARL-TR-4478

June 2008

Metastable Polymeric Nitrogen: The Ultimate Green High-Energy-Density Material

Jennifer A. Ciezak
Weapons and Materials Research Directorate, ARL

REPORT DOCUMENTATION PAGE			Form Approved OMB No. 0704-0188		
Public reporting burden for this collection of information is estimated to average 1 hour per response, including the time for reviewing instructions, searching existing data sources, gathering and maintaining the data needed, and completing and reviewing the collection information. Send comments regarding this burden estimate or any other aspect of this collection of information, including suggestions for reducing the burden, to Department of Defense, Washington Headquarters Services, Directorate for Information Operations and Reports (0704-0188), 1215 Jefferson Davis Highway, Suite 1204, Arlington, VA 22202-4302. Respondents should be aware that notwithstanding any other provision of law, no person shall be subject to any penalty for failing to comply with a collection of information if it does not display a currently valid OMB control number. PLEASE DO NOT RETURN YOUR FORM TO THE ABOVE ADDRESS.					
1. REPORT DATE (DD-MM-YYYY) June 2008		2. REPORT TYPE Final		3. DATES COVERED (From - To) October 2006–October 2008	
4. TITLE AND SUBTITLE Metastable Polymeric Nitrogen: The Ultimate Green High-Energy-Density Material			5a. CONTRACT NUMBER		
			5b. GRANT NUMBER		
			5c. PROGRAM ELEMENT NUMBER		
6. AUTHOR(S) Jennifer A. Ciezak			5d. PROJECT NUMBER DRI002		
			5e. TASK NUMBER		
			5f. WORK UNIT NUMBER		
7. PERFORMING ORGANIZATION NAME(S) AND ADDRESS(ES) U.S. Army Research Laboratory ATTN: AMSRD-ARL-WM-BD Aberdeen Proving Ground, MD 21005-5066			8. PERFORMING ORGANIZATION REPORT NUMBER ARL-TR-4478		
9. SPONSORING/MONITORING AGENCY NAME(S) AND ADDRESS(ES)			10. SPONSOR/MONITOR'S ACRONYM(S)		
			11. SPONSOR/MONITOR'S REPORT NUMBER(S)		
12. DISTRIBUTION/AVAILABILITY STATEMENT Approved for public release; distribution is unlimited.					
13. SUPPLEMENTARY NOTES					
14. ABSTRACT Fourier transform infrared and Raman studies were performed on a N ₂ /H ₂ mixture with a 2:1 ratio over a large pressure range (5–85 GPa) at room temperature in a diamond anvil cell. Based on the spectroscopic features observed within this pressure range and a thorough comparison to the vibronic modes of pure N ₂ and H ₂ , the vibrational spectra have been assigned. The difference between the infrared and Raman vibron frequencies for pure N ₂ and H ₂ relative to those observed in the N ₂ /H ₂ mixture is interpreted quantitatively with references to the possibility of new bonding arrangements or charge transfer between the components. High-pressure ultraviolet/visible electronic spectroscopy shows a broad absorption band that splits into two features near 30 GPa. The splitting of the absorption peak corroborates with the modifications that occur in the vibrational spectrum at similar pressures. Single-crystal x-ray diffraction studies were performed on the N ₂ /H ₂ complex to near 17 GPa, and the similarities to pure nitrogen as well as the limitations of the experiments are discussed.					
15. SUBJECT TERMS polymeric nitrogen, high pressure, diamond anvil cell, high-nitrogen compounds, novel energetic materials					
16. SECURITY CLASSIFICATION OF:			17. LIMITATION OF ABSTRACT	18. NUMBER OF PAGES	19a. NAME OF RESPONSIBLE PERSON
a. REPORT	b. ABSTRACT	c. THIS PAGE			Jennifer A. Ciezak
UNCLASSIFIED	UNCLASSIFIED	UNCLASSIFIED	UL	30	19b. TELEPHONE NUMBER (Include area code) 410-306-1904

Contents

List of Figures	iv
Acknowledgments	v
1. Introduction	1
2. Experimental Methodology	4
3. Results and Discussion	6
3.1 General	6
3.2 Vibrational.....	6
3.3 Electronic.....	13
3.4 X-ray Diffraction.....	13
3.5 Decompression Studies and Application to the Quest for Polymeric Nitrogen.....	15
4. Conclusion and Summary	16
5. References	17
Distribution List	21

List of Figures

Figure 1. Phase diagram of nitrogen.....	3
Figure 2. The optical system for UV-visible absorption measurements using a digital-to-analog converter. The use of quartz optical fibers, transparent to 5.5 eV, allows the optics to be very simple.....	5
Figure 3. Microphotographic images of the N ₂ /H ₂ alloy (all images were taken at room temperature). (a) The sample at 6.2 GPa showing the large single-crystal domains. (b) The sample at 30 GPa—in phase B, the sample is transparent while in phase A, the sample has a yellowish hue. The interface between the two regions is a dark-red/violet color. (c) The sample after a gradual pressure increase to 75 GPa. Two phases are still visible with an interface, which is less obvious than at lower pressures. The sample in phase A is reddish in color while the appearance of the sample in phase B remains virtually unchanged.....	7
Figure 4. Representative Raman spectra of the N ₂ /H ₂ sample are shown as a function of pressure. Spectral regions of interest are shown: (a) lattice vibrations, (b) nitrogen vibron, (c) N-H stretching, and (d) hydrogen vibron. At pressures below 30 GPa, spectra were obtained from the sample center, but above 30 GPa, spectra were obtained from phase B of the sample. The negative peak near 2550 cm ⁻¹ is an instrument artifact as is the positive peak at 83 GPa near 2575 cm ⁻¹	9
Figure 5. Representative Raman spectra taken from phase A (curve 1) and the boundary region (curve 2) at 34.6 GPa.....	11
Figure 6. Pressure dependence of the nitrogen vibron modes. Vertical lines indicate apparent phase boundaries.....	12
Figure 7. Pressure dependence of the hydrogen vibron modes. Vertical lines indicate apparent phase boundaries.....	12
Figure 8. Optical absorption spectra of the N ₂ /H ₂ complex.....	14

Acknowledgments

The author is grateful to the following researchers at the Geophysical Laboratory at the Carnegie Institution of Washington who provided assistance during the course of this research: Dr. T. Jenkins for help in preparing the N₂/H₂ mixture and for assistance in collecting the Raman spectra; Dr. M. Somayazulu for help with the x-ray and Raman measurements; and Dr. R. Hemley for valuable discussions over the course of this project. Dr. Z. Liu is thanked for his assistance in collecting the infrared measurements. These measurements were performed at the U2A beamline at the National Synchrotron Light Source of Brookhaven National Laboratory (U.S. Department of Energy [DOE] contract no. DE-AC02-98CH10886). The U2A beamline is supported by COMPRES, the Consortium for Materials Properties Research in Earth Sciences under the National Science Foundation (NSF) cooperative agreement grant no. EAR01-35554 and the Carnegie DOE Alliance Center contract no. DE-FC03-03N00144. Dr. P. Dera and Dr. H. Liermann are thanked for their assistance during the x-ray diffraction experiments. X-ray diffraction was performed at High-Pressure Collaborative Access Team (HPCAT) (sector 16), Advanced Photon Source (APS), Argonne National Laboratory. HPCAT is supported by the DOE Office of Basic Energy Sciences (DOE-BES), the DOE National Nuclear Security Administration, NSF, and the W. M. Keck Foundation. APS is supported by DOE-BES under contract no. DE-AC02-06CH11357. This work was supported by a U.S. Army Research Laboratory Director's Research Initiative.

INTENTIONALLY LEFT BLANK.

1. Introduction

In order to play a critical role in the U.S. Department of Defense (DOD) Joint Visions of 2010 and 2020, research and development communities within the DOD face an unprecedented challenge to transform the U.S. Army into a force that dominates the full spectrum of military operations. To satisfy these directives, there is an evolution toward smaller, lighter platforms that have increased range and lethality, which presents a daunting challenge for the development of future munitions. To meet the criteria required by the future force, new energetic materials (EMs) with enhanced stability, reduced sensitivity, and lower vulnerability are being aggressively pursued within the research community. There is a strong emphasis on materials that exceed both performance specifications and insensitive munitions requirements. An ideal candidate would also have a low environmental impact to satisfy the “green” munitions initiative. Novel energetic formulations are also of interest to this program as they offer mechanisms to tailor the dynamic release of energy, providing increased weapon efficiency and vulnerability while meeting the green munitions requirements.

The performance improvements offered by new EMs that have been formulated via the traditional synthesis route are rapidly becoming increasingly modest. In recent years, EMs with a higher nitrogen content than was used in previous formulations are being examined and tested due to the slight density increase. The crystalline density of energetic materials is often used as a benchmark indicator of material performance. Although these high nitrogen materials offer modest performance improvements, the exploitation of conventional synthesis methods to enhance the physical and chemical properties of even these high nitrogen materials is rapidly approaching a ceiling. In order to maintain the capability of the future force, new methods of synthesizing EMs must be investigated. Many simple diatomic and triatomic molecules such as N_2 , O_2 , and CO_2 have the potential to form extended molecular solids under extreme conditions, which, due to the bonding arrangements, have many times the energy of conventional EMs in use today. Diatomic nitrogen is particularly interesting because of the uniquely large energy difference between that of the single bond (160 kJ/mol) and that of the triple bond (954 kJ/mol). Under extreme conditions, nitrogen can, in theory, form a singly bonded polymeric network. If the polymeric nitrogen can be stabilized and isolated at ambient conditions, external stimuli can be tuned to cause detonation or burning. This back-conversion from a singly bonded material to diatomic nitrogen is highly exothermic in nature, and the corresponding energy release has been estimated at nearly five times the energy of any conventional EM (*1*).

Nitrogen, as the most strongly bonded simple diatomic, exists in several disordered and ordered molecular phases, even at moderate pressures (2–5). Nearly two decades ago, theoretical simulations indicated a transition to a nonmolecular phase in the pressure range accessible by modern experimental techniques (6–8). These predictions were confirmed when shock wave

experiments provided evidence for the nonmolecular transition in the liquid phase at 30 GPa and 6000 K (9). In spite of these earlier observations, it is only recently that any comparable transitions were observed using static measurements. Fundamentally, the lack of observed nonmolecular phases relates back to the strong intramolecular bonds, which make the molecular arrangement extremely stable. At high pressures, the intermolecular interactions change rapidly, and the molecular solids should undergo physical and chemical changes in order to modify their chemical bonding and to soften their stiff repulsive intermolecular potentials. Three mechanisms may occur at high pressures to delocalize electrons and soften repulsive potentials: (1) ionization, which creates attractive electrostatic energy, (2) polymerization, which leads to a delocalization of the intramolecular electrons between the neighboring molecules, and (3) metallization completely delocalizing electrons through conduction bands. Exploitation of these three mechanisms will lead to the appearance of novel materials that may have great potential as future EMs.

The known phase diagram of nitrogen is rather extensive (figure 1) and recent detailed experimental and theoretical investigations have substantially enhanced knowledge of the high-pressure behavior of nitrogen (7, 8, 10–24). Upon compression at room temperature, liquid nitrogen solidifies into the disordered β phase near 2 GPa (13). From the β phase, two low-temperature phases, α and γ , are accessible and primarily differ from other nitrogen phases in regards to the ordered quadrupole packing arrangements (14). The quadrupoles are not ordered in the δ , δ_{loc} , ϵ , and ζ high-pressure phases (2, 3, 10, 15, 16). The disordered δ phase has sphere and disc-like atoms orientationally distributed between the corners and faces of the *fcc* cell (2). With increasing pressure and/or decreasing temperature, partial ordering of the molecules occurs in the δ_{loc} phase, while complete ordering develops in the ϵ -N₂ phase. Theoretical simulations confirm the ordered stability of the ϵ phase between 2 GPa and 40 GPa (17), although some simulations favor tetragonal structures (18) that are in contrast with the experimental data available at these pressures. Further increases in pressure lead to a phase transformation to the ζ -N₂ phase. At low temperatures, this phase transition is quite pronounced (10), but only subtle vibrational changes (2, 11) are observed at room temperature. Above 115 GPa, recent experiments indicate the ζ phase transitions to the κ -N₂ phase (19). The two phases have similar structures as evidenced by Raman spectroscopy (2, 11, 20); both result from a lowering of the ϵ symmetry. The κ -N₂ phase is the densest phase observed prior to the transformation to the nonmolecular η phase. At 130 GPa, nitrogen transforms into the η phase, which is believed to be similar to the high-pressure singly bonded polymeric cubic gauche phase but with crystalline defects (19).

Although extensive characterization of the nitrogen phase diagram exists, until recently, there was no convincing data for any nitrogen phase with an extended polymeric network, including the cubic gauche structure (*cg*-N). In 2004, Eremets et al. reported the first successful synthesis of the *cg*-N phase directly from molecular nitrogen (21). Diatomic nitrogen was subjected to temperatures above 2000 K and pressures above 110 GPa, and characterized using powder x-ray

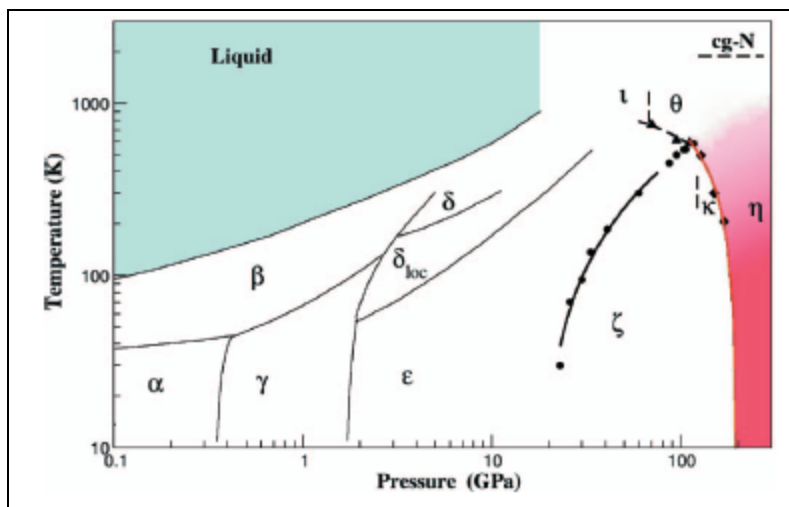


Figure 1. Phase diagram of nitrogen.

diffraction and Raman spectroscopy (21). The limited number of x-ray diffraction peaks precluded confirmation of the *cg-N* structure until recently, when single-crystal x-ray diffraction confirmed the structure (22). A transformation from the molecular to the nonmolecular *cg-N* phase was observed at pressures above 110 GPa; the accumulation of defects in the crystalline lattice that accompanies this phase transition leads to increased sample luminescence (22). After the sample is heated to 2000 K, the nitrogen transforms to a nonmolecular phase with the characteristic *cg-N* Raman peak at 820 cm^{-1} . A large pressure drop accompanies the phase transition, which ranges between 5 and 20 GPa depending on the sample temperature, indicating a significant reduction in the sample volume. Although the *cg-N* phase has been isolated at low temperatures at ambient pressure, it has yet to be stabilized at both ambient pressure and temperature (21, 22), thus precluding any testing of its performance characteristics.

There has been extensive theoretical debate about the stability of nonmolecular polymeric phases of nitrogen at ambient conditions, particularly the *cg-N* phase (25). Quantum mechanical (QM) calculations have characterized and tested the stability of high-pressure, nonmolecular amorphous structures generated through quenching hot atomic nitrogen gas. Upon decompression, the polymeric structures become destabilized when adjacent singly coordinated atoms within the nitrogen network break away to form diatomic molecules (26). This “unraveling” of the polymeric structure propagates through the polymer and ultimately results in a back transformation to a molecular phase. QM calculations have shown that passivation of the terminal ends of the singly coordinated atoms with an impurity, such as hydrogen or ammonia, produced an increase in the stability of the amorphous polynitrogen structures upon decompression (27). Additionally, the simulations have indicated that a N_2/H_2 mixture with a 2:1 ratio would be ideal in promoting polymer metastability at ambient conditions. Isolating a metastable form of polymeric nitrogen is an important first step in determining both its performance as an EM and its stability in weapons platforms.

Using these quantum mechanical simulations as a guide, an experimental investigation has been conducted into the feasibility of stability enhancement, at ambient conditions, of the polymeric form of nitrogen employing a 2:1 N₂/H₂ mixture (for simplicity, this mixture will be referred to as the N₂/H₂ sample throughout the remainder of the report). The binary mixing of two molecular systems in the hope of stabilizing the materials into ordered solid phases is still quite novel, having been employed to only a few systems (27–30). These are, under all respects, new compounds where the molecules are held together by weak van der Waals forces, which result in the stabilization of entirely different structures than those typically observed in the pure molecular solid. The N₂/H₂ sample was studied as a function of pressure to 85 GPa employing Raman and infrared (IR) spectroscopy, electronic ultraviolet/visible (UV/vis) spectroscopy, and x-ray diffraction. To near 30 GPa, there are strong correlations between the spectral data of the solid N₂/H₂ sample and pure N₂ and H₂. Above 30 GPa, the behavior of the N₂/H₂ sample begins to deviate from the known behavior of N₂ and H₂, and it becomes increasingly evident that chemical interactions are occurring.

2. Experimental Methodology

Nitrogen and hydrogen gas were mixed using a specialized gas chamber (31) in the ratio of ~66% N₂ to ~33% H₂. The gaseous sample thermally equilibrated for one week at room temperature before use. The gas was then loaded into the diamond anvil cell using the gas chamber (31). Optical measurements consisting of Raman, synchrotron-based IR, and UV/vis spectroscopies were measured to pressures near 80 GPa at room temperature. The pressure on the sample was determined from the frequency shift of the R₁ fluorescence line (32). The Raman excitation radiation was an argon-ion laser (Coherent Innova 90) operating at 514 nm with a power of 0.5 W and a laser spot size of ~7 μm in diameter. A 460-mm focal length f/5.3-imaging spectrograph (ISA HR 460) equipped with an 1800-groves/mm grating, which provides a spectral resolution of ±4.0 cm⁻¹, was used for all Raman experiments. Prior to any experimental measurements, a wavelength calibration of the spectrograph was performed with a neon lamp; this method of calibration has an accuracy of ±1.0 cm⁻¹ (33). Synchrotron IR-absorption experiments were performed at beamline U2A of the National Synchrotron Light Source of Brookhaven National Laboratory. The synchrotron light is extracted from the vacuum ultraviolet storage ring in a 40 × 40-mrad solid angle. The collimated beam is delivered through a vacuum pipe system and directed into a Bruker IFS 66v Fourier transform infrared spectrometer. Extensive detail of the optical layout of this beamline is available (34). The resolution used for all measurements was 4 cm⁻¹.

Optical absorption measurements were collected from the mid-UV to the near-IR spectral ranges. The instrumental configuration used for the UV-vis measurements are shown in figure 2. The

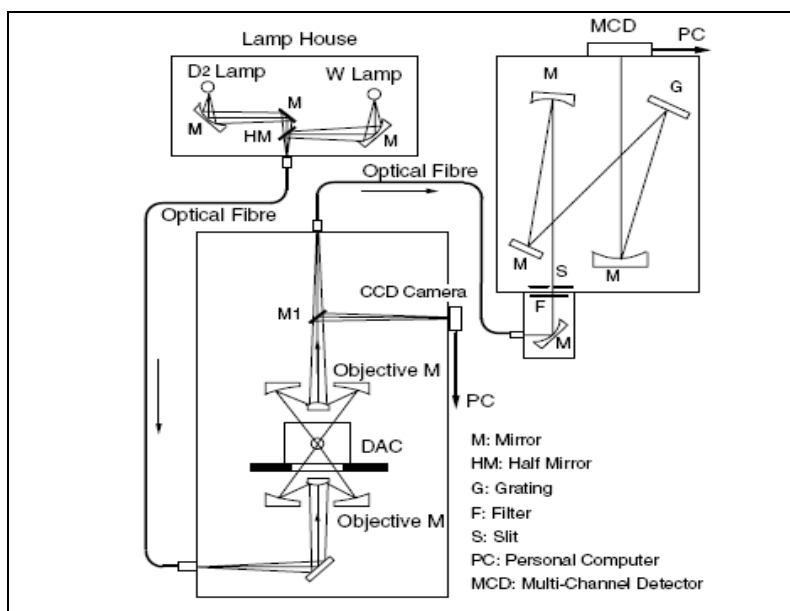


Figure 2. The optical system for UV-visible absorption measurements using a digital-to-analog converter. The use of quartz optical fibers, transparent to 5.5 eV, allows the optics to be very simple.

use of quartz optical fibers, which are transparent to 5.5 eV, permits a very simple optical layout. The optical fibers for input and output are typically 50 and 800 μm in core size, respectively. The white light from the 50- μm fiber is focused onto the sample using a reflective objective without chromatic aberration. The other reflecting objective focuses the transmitted light onto the 800- μm fiber connected to a single monochromator. The images of the sample and the illuminated spot can be monitored with a charge-coupled device camera. The diameter of the focused spot, which depends on the size of the optical fiber used, was about 30 μm smaller than the sample chamber. The white light source covering a wide spectral range was achieved by the combination of a deuterium lamp and a tungsten lamp. To deduce the absorption spectra of the specimen itself, the absorption of the diamond as well as the empty cell were measured prior to the loading of the sample. The resulting spectra were then used to normalize the spectrum of the sample.

X-ray diffraction techniques are essential for the characterization of high-pressure phases. Energy-dispersive single-crystal x-ray diffraction was performed at beamline 16BM-B (HPCAT) at the Advanced Photon Source of Argonne National Laboratory (35). The sample-to-detector distance was calibrated using a National Institute of Standards and Technology CeO_2 standard. The beam was focused to 20 μm (horizontal) by 20 μm (vertical) by two platinum-coated, 300-mm-long electrode bimorph mirrors and then guided by a pinhole mounted at the end of 3-mm-diameter tubes before incident into the diamond anvil cell. The sample position relative to the beam center was corrected in y , z , ω , and χ . A peak search was performed with an omega range of $\pm 10^\circ$ and 360° in χ . An orientational matrix was generated from the experimentally

determined list of peaks using the Reciprocal Space Viewer (RSV) program, without making any assumptions of the unit cell parameters of the measured crystal (36). The RSV program (36) employs an indexing method based on the analysis of most frequent difference vectors. The most frequent difference vectors were calculated from the N₂/H₂ sample, and the indexing parameters were independently optimized to ensure a best fit of the data. Based on this peak fitting analysis, a unit cell was selected and lattice parameters were derived. After initial lattice parameters were defined, the lattice parameters were refined to minimize the error.

3. Results and Discussion

3.1 General

Upon loading the N₂/H₂ mixture in the cell, it was difficult to maintain the hydrogen within the cell unless the pressure was raised to 6 GPa, which is slightly above the freezing point of hydrogen (5.5 GPa [37]). This behavior is quite common in gaseous hydrogenous samples because the hydrogen escapes through small microcracks in the diamond anvils. Solidification of the N₂/H₂ sample becomes visually apparent near 6 GPa, as several large, translucent single crystals appear with well-defined grain boundaries (figure 3a). Preservation of the single crystals was possible to near 17 GPa with slow increases in pressure. Slightly above 17 GPa, a reconstructive phase transition occurred, and the single crystals were lost. Visual inspection of the polycrystalline sample upon further pressure increase revealed a phase separation begins near 28 GPa and is completed near 30 GPa. Near 30 GPa, figure 3b shows phase A is translucent and light yellow in color, and phase B is transparent with a dark-reddish/black well-defined interface. As pressure is increased to 83 GPa, the distinct phase boundaries present at lower pressures become less obvious. The yellow color of phase A darkens into a deep red, which resembles the interface at lower pressures. At this high pressure, a change in color typically signifies modification in the electronic structure, such as band gap closure or a change in the conjugation structure of the bonds, both of which will be discussed in greater detail later in the report. Phase B remains translucent to the highest pressure studied (83.3 GPa). Upon decompression, the heterogeneity of the sample visually disappeared near 50 GPa. Interestingly, the hydrogen component could be maintained in the cell at very low pressures once the sample had been compressed and then decompressed. Using this technique, an N₂/H₂ sample was maintained at 0.5 GPa for over 6 months without any change in the chemical composition.

3.2 Vibrational

Close correlations exist, at least to 30 GPa, between the Raman spectral signatures of the N₂/H₂ mixture and those of pure nitrogen and hydrogen. Although the spectral intensity is weak, figure 4 reveals several broad bands that can be attributed to the nitrogen lattice modes and the rotational bands of the hydrogen. The large linewidth of these features indicates the disorder in

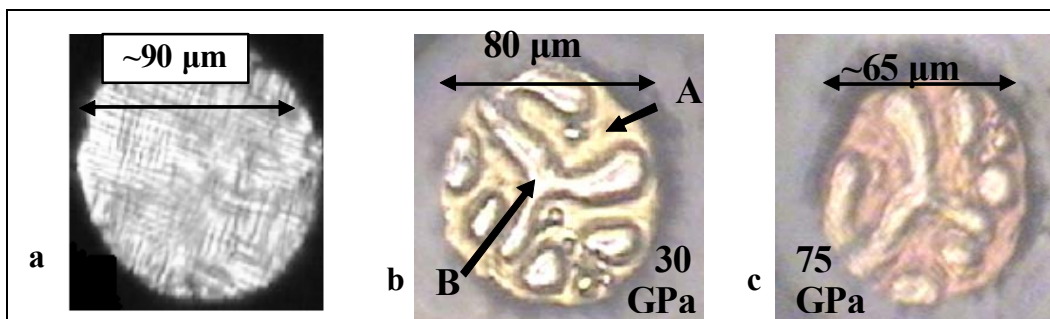


Figure 3. Microphotographic images of the N_2/H_2 alloy (all images were taken at room temperature). (a) The sample at 6.2 GPa showing the large single-crystal domains. (b) The sample at 30 GPa—in phase B, the sample is transparent while in phase A, the sample has a yellowish hue. The interface between the two regions is a dark-red/violet color. (c) The sample after a gradual pressure increase to 75 GPa. Two phases are still visible with an interface, which is less obvious than at lower pressures. The sample in phase A is reddish in color while the appearance of the sample in phase B remains virtually unchanged.

the system caused by the presence of the second component. The appearance of two nitrogen lattice modes ca. 200 and 400 cm^{-1} at 7.5 GPa is in close agreement with previous spectral measurements of the δ - N_2 phase, in which three of the four lattice modes predicted by group theory were observed (38). As in the previous study, the broad features preclude the identification of the remaining nitrogen lattice modes. Spectral signatures associated with the hydrogen rotational bands are also observed and, although weak in intensity, the assignment of these bands is rather straightforward: (1) $\sim 300\text{ cm}^{-1}$ $J_0 \rightarrow J_2$ (Para- H_2), (2) $\sim 600\text{ cm}^{-1}$ $J_1 \rightarrow J_3$ (Ortho- H_2), (3) $\sim 800\text{ cm}^{-1}$ $J_2 \rightarrow J_4$ (Para- H_2), and (4) $\sim 1100\text{ cm}^{-1}$ $J_3 \rightarrow J_5$ (Ortho- H_2) (37, 39). The appearance of these modes indicates that at low pressure, the H_2 component of the N_2/H_2 mixture can perform almost free rotations and vibrations, similar to observations noted in free hydrogen. The similarities in the spectral positions of these rotational modes for the mixture and pure H_2 indicate the rotational energy levels are only slightly displaced from that of the free molecule. Previous spectroscopic studies have shown these rotational hydrogen modes are rather intense (38–39), but in the case of the N_2/H_2 mixture, several factors contribute to the low intensity, such as (1) the disorder in the system, (2) the small amount of hydrogen in the sample, and (3) the inhomogeneity of the sample at lower pressures, which may result in small pockets of hydrogen.

The vibrational spectrum provides strong evidence that the reconstructive phase transition near 18 GPa is the $\delta \rightarrow \epsilon$ phase transition also observed in pure N_2 . Weak N_2 lattice vibrations at 243, 267, and 351 cm^{-1} are noted in the Raman spectrum at considerably lower frequencies than in pure N_2 (38). The shift in the nitrogen lattice modes to lower frequencies coupled with the shift in the hydrogen rotational bands toward higher energy indicates significant perturbation of the vibrational energy levels and intermolecular potential energies of both systems. The modifications in the intermolecular interactions and their subsequent effect on the vibrational energy levels become increasingly apparent in the Raman spectra as the pressure continues to increase; the Raman signatures apparent at lower pressure gradually disappear between 18 and

35 GPa and culminate to a virtually featureless Raman spectra near 35 GPa, which accompanies the unusual phase transition/separation (figure 3). Both phase A (figure 4) and phase B (figure 5, curve A) show little Raman activity in this spectral range near 35 GPa, but the purplish/red interface shows slightly increased activity near 600 and 900 cm^{-1} (figure 5, curve B). Previous studies have shown that these low-frequency modes arise from bending (600 cm^{-1}) (23) and stretching (900 cm^{-1}) (21, 22, 40) activity from single-bonded nonmolecular phases of nitrogen. Because it became increasingly difficult to sample purely from the interface with subsequent increases in pressure, phase B was sampled in close proximity to the interface, which resulted in a spectra where the spectral signatures from both phase B and the interface were averaged. Phase A showed no additional Raman features with subsequent pressure increases and showed strong photoluminescence with the 514.5-nm laser beam, similar to observations of Lipp et al. (40) for the amorphous η phase.

With increasing pressure, the differences between the lower-pressure phases and the high-pressure phase become increasingly apparent. A new, broad lattice mode emerges ca. 300 cm^{-1} near 51 GPa, and the N-N modes at $\sim 625 \text{ cm}^{-1}$ (bending) and 925 cm^{-1} (stretching) are considerably stronger in intensity and slightly shifted to higher frequency. Between 51 and 83 GPa, a second lattice mode appears on the high-frequency side of the lattice mode, and the modes near 650 and 950 cm^{-1} become rather intense. It is expected that as more of the nitrogen within the N_2/H_2 phase is converted to the nonmolecular phase, the intensity of these modes will continue to increase. The correlation between the intensity of these modes and the amount of N-N phase present is supported by the changes in the color over this pressure range in phase B. Previous experiments have correlated the red color to an increase in conjugation from the $\text{N}\equiv\text{N}$ bonding structure to the $-\text{N}=\text{N}-\text{N}=\text{N}-$ type structure (40) and have proposed that this intermediate structure is a precursor to the singly bonded phase. However, the presence of both the nitrogen and hydrogen vibrons (figure 4) show that even at 83 GPa, conversion to a N-N-type structure is not yet complete.

At the highest pressures studied, phase B showed enhanced activity between 3300 and 3600 cm^{-1} (figure 4), which is typically the spectral range associated with N-H stretching. Although the broad mode ca. 3450 cm^{-1} in figure 4 has a spectral position similar to the antisymmetric stretching mode of ammonia (41), the inconsistencies between the other spectral features provide strong evidence that the phase in phase B is not ammonia. Since the vibrational mode observed in this spectral range shifts to a higher frequency with increasing pressure, it is also unlikely that this novel phase exhibits hydrogen bonding; typically, the frequencies of hydrogen-bonded materials shift to lower frequencies with increasing pressure (41).

The nitrogen vibrons of the N_2/H_2 mixture closely resemble the vibronic signatures of pure N_2 , at least to 30 GPa, except the vibrons for the N_2/H_2 mixture appear at much lower frequencies. Figure 6 shows with increasing pressure the two vibronic branches, ν_1 (2393 cm^{-1}) and ν_2 (2348 cm^{-1}), observed at a 7.5-GPa shift to higher frequencies; the frequency shift is slightly

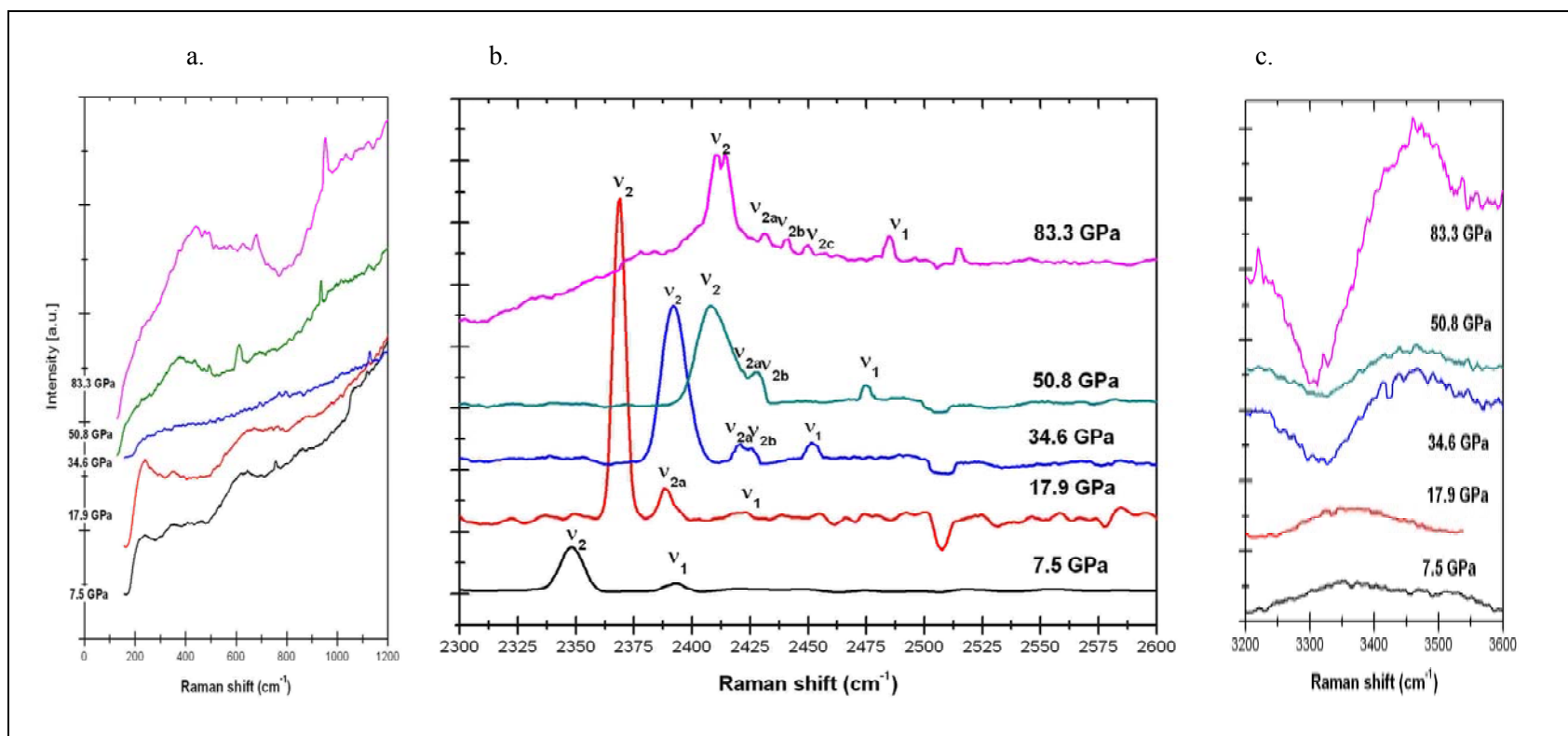


Figure 4. Representative Raman spectra of the N₂/H₂ sample are shown as a function of pressure. Spectral regions of interest are shown: (a) lattice vibrations, (b) nitrogen vibron, (c) N-H stretching, and (d) hydrogen vibron. At pressures below 30 GPa, spectra were obtained from the sample center, but above 30 GPa, spectra were obtained from phase B of the sample. The negative peak near 2550 cm⁻¹ is an instrument artifact as is the positive peak at 83 GPa near 2575 cm⁻¹.

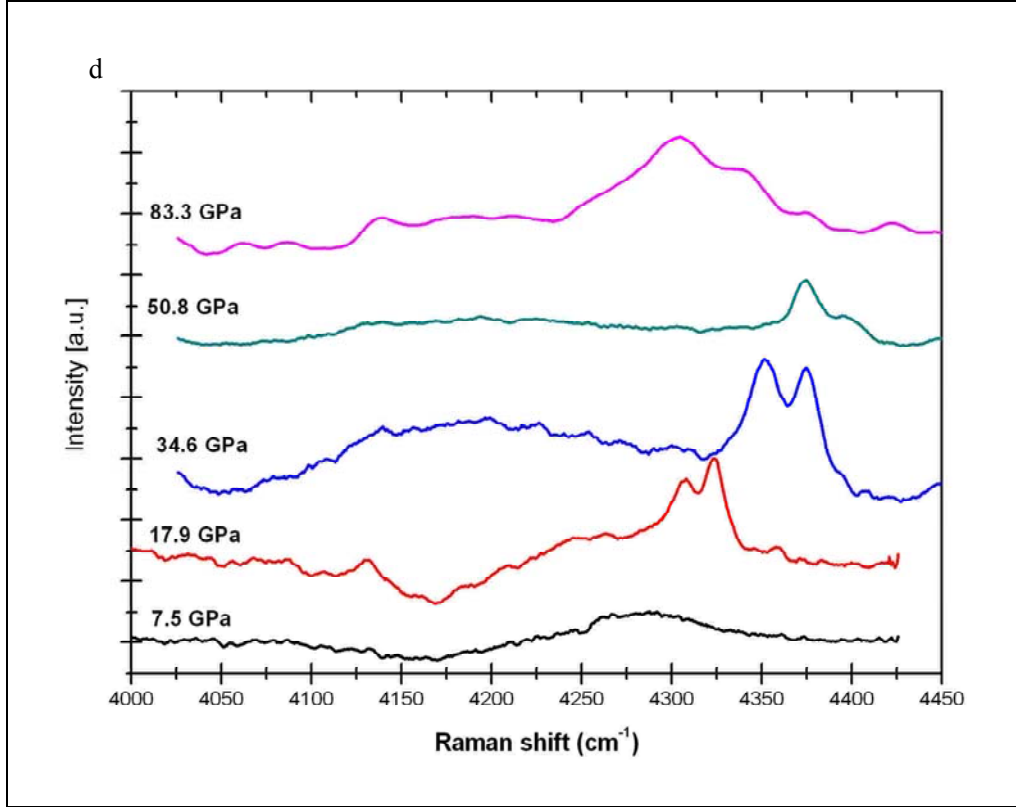


Figure 4. Representative Raman spectra of the N_2/H_2 sample are shown as a function of pressure. Spectral regions of interest are shown: (a) lattice vibrations, (b) nitrogen vibron, (c) N-H stretching, and (d) hydrogen vibron. At pressures below 30 GPa, spectra were obtained from the sample center, but above 30 GPa, spectra were obtained from phase B of the sample. The negative peak near 2550 cm^{-1} is an instrument artifact as is the positive peak at 83 GPa near 2575 cm^{-1} (continued).

more pronounced for ν_2 . The intensity ratio of the modes is similar to that of pure N_2 ($\sim 3:1$), which suggests the distribution of the molecules is nearly the same as in $\delta\text{-}N_2$. Consistent with the $\delta \rightarrow \epsilon$ phase transition of pure N_2 , a new vibron (ν_{2a}) appears on the high-frequency side of the ν_2 peak in the N_2/H_2 spectrum near 18 GPa. The ϵ phase has a rhombohedral lattice (R-3c) derived from the cubic- δ lattice, and the Raman active modes consist of one branch of A_{1g} symmetry associated with the corner and body-centered molecules and one branch of A_{1g} and E_g symmetry modes associated with the face molecules. Increased factor group splitting and removal of the E_g degeneracy can explain the triplet vibronic structure, which persists to near 30 GPa. Gradual spectral changes occur at pressures above the phase transition that deviate from known N_2 spectral signatures. Slightly above the phase transition, there is nearly a factor-of-2 decrease in the ν_2 intensity, and there is an increase in the full width half maximum (FWHM). The intensity of this mode decreases further between 35 and 51 GPa but remains nearly constant between 51 and 83 GPa. The intensity decrease can be explained by partial conversion of the $N\equiv N$ structure to that of a double or singly bonded structure, while an increase in the FWHM might simply reflect changes in the site symmetry of the molecule. The appearance of new

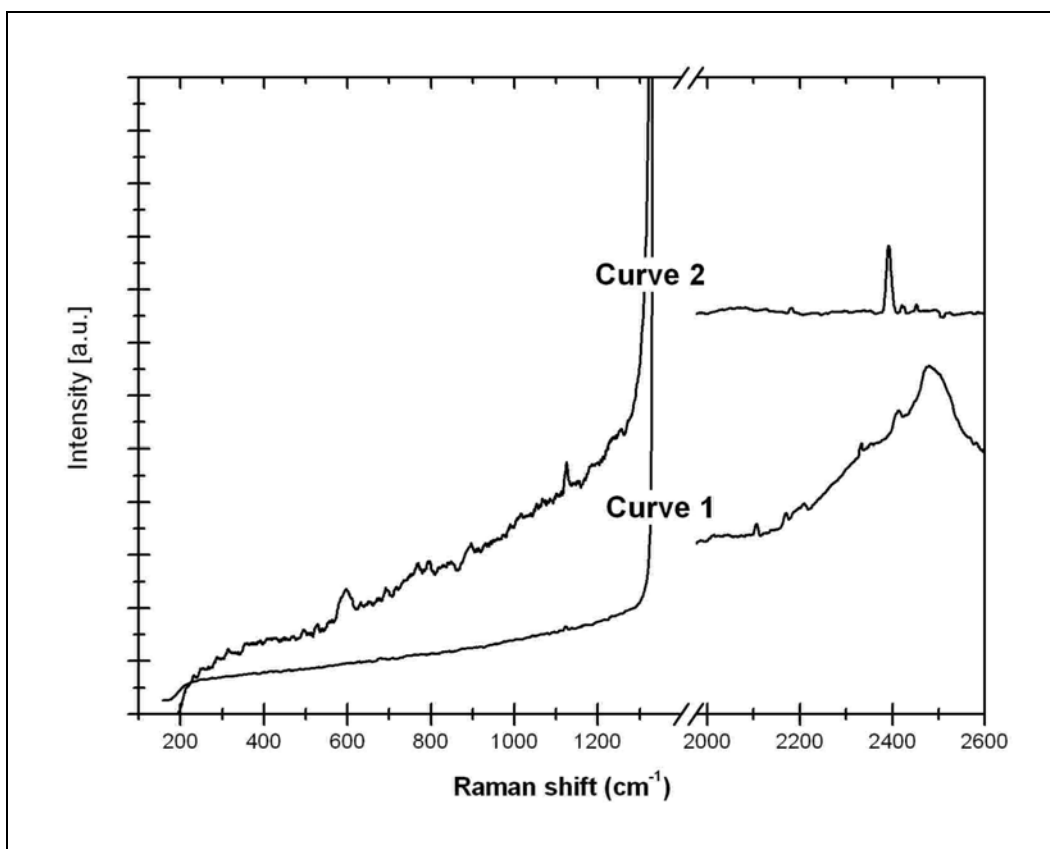


Figure 5. Representative Raman spectra taken from phase A (curve 1) and the boundary region (curve 2) at 34.6 GPa.

vibrons on the high-frequency side of ν_2 near 35 GPa supports the modifications in site symmetry as these likely arise from factor group splitting. At 83 GPa, five vibrational features are clearly resolvable, and there is a splitting of ν_2 into a doublet. Interestingly, there is also a slight downshift in frequency for ν_1 , ν_{2a} , and ν_{2c} (figure 6), which signifies the large changes occurring in the intermolecular interactions.

The hydrogen component of the N_2/H_2 sample also shows vibron frequencies (figure 7), although the number of vibronic modes and the frequencies differ from those of all other known molecular species. At pressures near freezing, the large FWHM of the hydrogen vibron provides evidence for disorder. As pressure is increased, near 18 GPa the fundamental vibron splits into two well-defined maxima. Three possible causes are proposed to explain this behavior. First and most likely, the restriction on the higher-frequency IR mode may be removed, due to a strong decrease in the crystal quality or to a phase transition to a lower-symmetry cell. Second, there may be phase separation of the hydrogen, where one phase acts as almost free hydrogen while the other is complexed to the nitrogen component. Finally, the high- and low-frequency vibrons may be attributed to the $Q_1(0)$ (para- H_2) and $Q_1(1)$ (ortho- H_2) transitions, respectively. However, this splitting has not been previously observed in the room temperature Raman spectrum due to motional narrowing (42). Between 51 and 83 GPa, vibron softening is observed and continues to

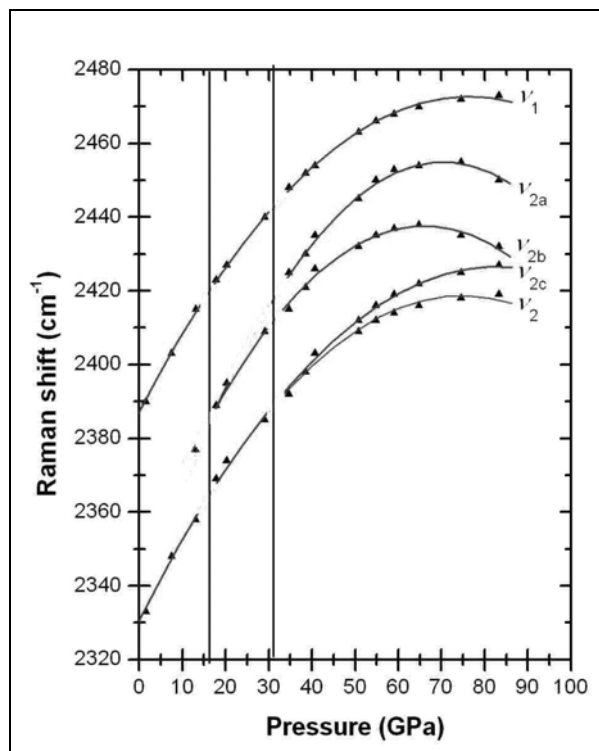


Figure 6. Pressure dependence of the nitrogen vibron modes. Vertical lines indicate apparent phase boundaries.

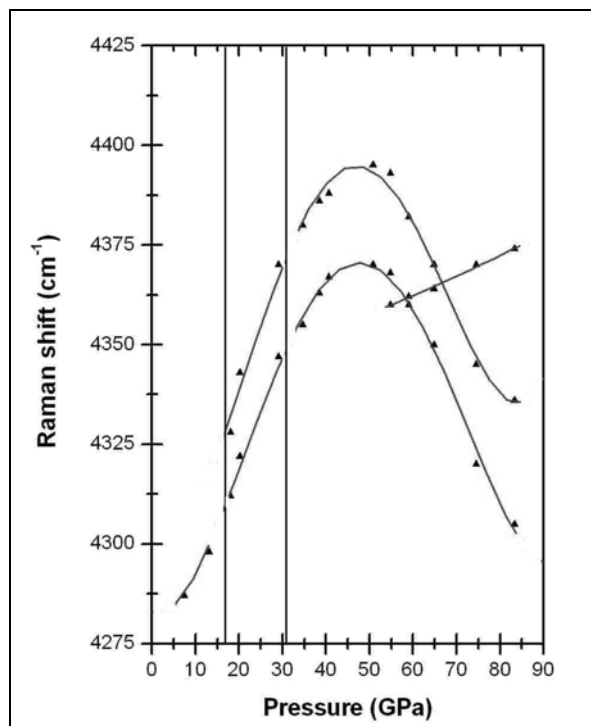


Figure 7. Pressure dependence of the hydrogen vibron modes. Vertical lines indicate apparent phase boundaries.

the highest pressure studied. These frequencies soften at a much slower rate than in pure hydrogen. Near 51 GPa, a new vibration appears in this spectral region ca. $\sim 4355\text{ cm}^{-1}$, which shifts to a higher frequency as pressure increases. Given the low spectral intensity and the large linewidth of this vibration, it is suspected to arise from an overtone.

3.3 Electronic

In the ground state, N_2 has 10 electrons arranged in the electronic configuration $1\sigma^2 1\sigma^{*2} 2\pi_x^2 2\pi_y^2$ while H_2 has the electronic configuration of $1\sigma^2$. As pressure is increased and new materials are formed, shifts in the electronic structure are expected. The electronic configuration of nitrogen, with its low-lying π molecular orbitals, makes it an ideal candidate for pressure-induced electronic transitions.

Selected UV/vis electronic absorption spectra of the N_2/H_2 complex to slightly above 74 GPa are shown in figure 8. Below 5 GPa, the sample is translucent, but with increasing pressure, an absorption band appears near 6 GPa. The appearance of this absorption band presumably relates to the sample solidification and is known to primarily arise from the nitrogen component of the complex (43). As pressure nears 30 GPa, the intensity of the absorption band increases, and the peak becomes increasingly broad with a tail toward lower energy. The broadening of this band correlates with the phase separation shown in figure 3 as well as notable changes in the vibrational spectra. Near 30 GPa, a new band appears on the low-energy side of the original band. Slightly above this pressure, a new, broad Raman-active vibrational band appears in the spectral region between 3350 and 3600 cm^{-1} . The coincidence of these two features in the electronic spectrum and the vibrational spectrum suggests charge transfer occurs between the nitrogen and hydrogen component. The intensity of this new electronic feature grows gradually with pressure and finally dominates over the original band at high pressures. As pressure increases, the lower-energy peak shifts toward lower energy, presumably caused by the shift in the intermolecular forces, as the electrostatic attractive forces become dominant over the repulsive forces. The shift in the band to lower energy may also relate to band gap closure and closely resembles that of a semiconductor (44), but further experimental characterization must be done to confirm this. Between 64 and 74 GPa, a shoulder appears toward lower energy. This feature may be another electronic transition, but it is more likely that this shoulder corresponds to the stress in the diamonds (45).

3.4 X-ray Diffraction

X-ray diffraction of low-elemental materials, such as nitrogen and hydrogen, is very difficult due to the low x-ray-scattering cross section. Under high-pressure conditions, experimental measurements are hampered further by a variety of limitations, such as scattering angle and sample size. However, with the commissioning of beamline 16-BM-B in early spring 2007, it has become possible to resolve single-crystal x-ray diffraction patterns to obtain unit cell vectors. This process is still very complicated and difficult; as a result, only two unit cells were resolved over the course of this Director's Research Initiative, although further experiments are planned.

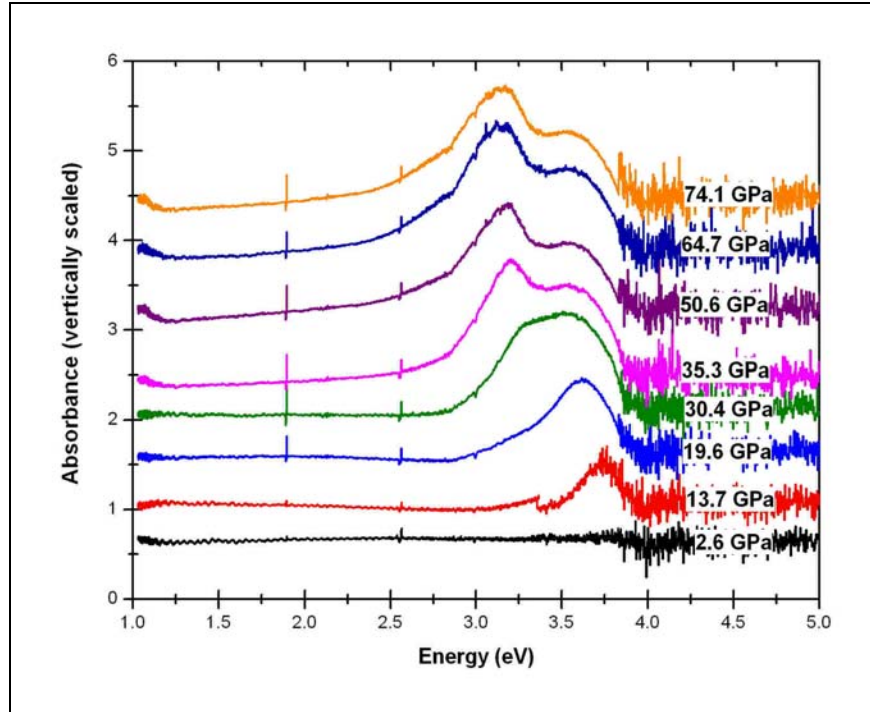


Figure 8. Optical absorption spectra of the N_2/H_2 complex.

Although the information gained by this technique is limited, when coupled with the spectroscopic and electronic data it provides valuable insight into the phase behavior of this material.

X-ray diffraction patterns of the N_2/H_2 complex measured in the stability field of $\delta\text{-N}_2$ agree with previous studies (19, 20, 46) (see figure 1). At 7.1 GPa, the material was found to be cubic with $a_0 = 5.97(3)$ Å and a space group of $Pm\bar{3}n$, similar to $\delta\text{-N}_2$. During these experiments, information regarding the hydrogen phase was unresolved due to the small size of the crystallites. At 12 GPa, x-ray diffraction data started to show an asymmetry and a generalized broadening of peaks that is inferred to correspond to the $\delta \rightarrow \delta_{\text{loc}}$ phase transition. In contrast to previous x-ray diffraction results (5), x-ray patterns were indexed and refined using a primitive cubic cell with $a = 5.831(5)$ Å, $b = 5.934(8)$ Å, $c = 5.829(5)$ Å, $\alpha = 89.34(1)^\circ$, $\beta = 90.17(4)^\circ$, and $\gamma = 90.10(1)^\circ$. The deviation of the unit cell observed at this pressure from the typical cubic cell where $a = b = c$ and $\alpha, \beta, \gamma = 90^\circ$ is caused by several factors.

- Due to the disorder in the δ_{loc} phase of nitrogen, the crystal is not exactly cubic. However, the cubic space group indexes the x-ray diffraction pattern better than the earlier-proposed tetragonal $P4_2/nm$ structure (5). A cubic structure also adequately explains the spectroscopic signatures (20).
- In all high-pressure experiments, some degree of stress/strain exists regardless of the hydrostaticity of the sample. In this case, the a and c unit cell vectors are very similar

while the b vector slightly deviates. In the configuration used for this experiment, the b vector is parallel to the compression axis, most likely resulting in the deviation.

- The sample studied was not very well crystallized. Unlike normal single-crystal experiments with one large single-crystal, there were many small, randomly oriented single crystals present. The random orientation and various crystal sizes may have resulted in some averaging of the lattice vectors. In future experiments, the cell will be heated to induce better crystallization.

Above 16 GPa, the phase diagram shows a transition from the $\delta_{\text{loc}} \rightarrow \epsilon$ phase. Spectroscopic data suggest the N_2/H_2 material follows the same phase pattern of pure nitrogen at these low pressures. Several attempts were made to perform single-crystal diffraction experiments to confirm the vibrational results, but the phase transition was reconstructive and the crystals were crushed during the pressure increase. Typically, in high-pressure experiments, single crystals are reformed after the phase transition by heating. Unfortunately, the configuration of the cell used for these experiments did not permit heating. Future experiments will be conducted using a cell designed for experiments where sample heating is required.

3.5 Decompression Studies and Application to the Quest for Polymeric Nitrogen

Decompression studies were undertaken using both vibrational and electronic spectroscopy to investigate the stability of the N_2/H_2 complex at ambient conditions. As was described previously, visual inspection suggests the nonmolecular material formed at high pressures backtransforms to the starting materials at lower pressures. Even if back transformation occurs on a macroscopic scale, microscopically transformed nonmolecular material, which is possibly polymeric, may exist within the large sample.

The vibrational and electronic data collected upon decompression from 85 GPa is a bit misleading. Both the nitrogen and hydrogen vibrons follow the projected decompression pattern derived from the compression results. However, at the lowest decompression pressure studied (7.5 GPa), the vibrons are shifted nearly 30 cm^{-1} to higher energy. The electronic spectra show similar decompression patterns, but the intensity of the absorption peak is much stronger than the original peak. These results suggest that back transformation of the N_2/H_2 material is complex, and multiple phases could exist. Further studies are certainly warranted on this unique behavior to derive a better understanding.

The experiments detailed in this report lay an important foundation for future work concerning this complex. Difficulty arises when attempting to isolate the transformed nonmolecular, and possibly polymeric, material at ambient conditions because both components are gases at standard temperature and pressure. This alone precludes any performance testing. Yet in contrast to polymeric nitrogen, which was only synthesized by heating to 3000 K at pressures of 150 GPa, the results from the N_2/H_2 complex suggested formation of a nonmolecular phase as low as 30 GPa at room temperature. This fact alone highlights the importance of these

experiments in polymeric nitrogen research. Future experiments will investigate the material under a wider range of conditions, such as high temperature and pressure, in an attempt to cause an irreversible phase transition that will permit the successful isolation of the material at ambient conditions.

4. Conclusion and Summary

These results provide important insights into the behavior of the N_2/H_2 complex at high pressures and room temperature. The sample appears to behave similar to pure N_2 to near 30 GPa and slightly different above 30 GPa to the highest pressure studied near 85 GPa. Below 30 GPa, the N_2/H_2 phases spectroscopically resemble the lower-pressure δ , δ_{loc} , and ϵ polymorphs of pure N_2 . X-ray diffraction confirmed the presence of both the δ and δ_{loc} phases near 7 and 13 GPa, respectively. Slightly above 30 GPa, a phase that vaguely displays spectroscopic signatures similar to a nonmolecular single-bonded phase appears. The strikingly different vibrational energies between the N_2/H_2 complex and pure N_2 indicate that the former is characterized by strong intermolecular interactions. Two rather broad peaks were observed in the Raman and IR spectral regions typically associated with N-H bonding, but the large peak in the electronic data suggests charge transfer occurs rather than N-H bonding. If the interactions are strong enough to cause charge transfer, the phase may be related to theoretically predicted polyatomic species (48), but this requires further investigation. Decompression experiments gave rather complicated results, and additional analysis is required before any definitive conclusions can be gathered from these experiments. However, it was shown that the high-pressure nonmolecular phase of the N_2/H_2 complex is retained in small quantities to near 7 GPa. An important general conclusion of this work is that the definitive determination of the equilibrium phase relations of nitrogen is more complex than previously thought due to substantial transformation barriers between different structures. Although unique chemistry has been observed in the N_2/H_2 complex, it remains to be seen whether the hydrogen component can introduce a stabilizing effect onto the polymeric nitrogen network. Additional experiments are required to investigate the thermodynamic stability of the proposed N_2/H_2 phases over a wider range of extreme conditions in the hope of promoting stability in the polymeric structure.

5. References

1. Ritter, S. Polynitrogen. *Chem. Eng.* **2004**, *82*, 10.
2. Cromer, D. T.; Mills, R. L.; Schiferl, D.; Schwalbe, L. A. The Structure of N₂ at 49 kbar and 299K. *Acta Crystallogr.* **1981**, *B37*, 8.
3. Mills, R. L.; Olinger, B.; Cromer, D. T. Structures and Phase Diagrams of N₂ and CO to 13 GPa by X-ray Diffraction. *J. Chem. Phys.* **1986**, *84*, 2837.
4. Olijnyk, H. High Pressure X-Ray Diffraction Studies on Solid N₂ up to 43.9 GPa. *J. Chem. Phys.* **1990**, *93*, 8968.
5. Hanfland, M.; Lorenzen, M.; Wassilew-Ruel, C.; Zontone, F. *Rev. High Pressure Sci. Technol.* **1998**, *7*, 787.
6. McMahan, M. K.; Lesar, R. Pressure Dissociation of Solid Nitrogen Under 1 Mbar. *Phys. Rev. Lett.* **1985**, *54*, 1929.
7. Martin, R. M.; Needs, R. J. Theoretical Study of the Molecular-to-Nonmolecular Transformation of Nitrogen at High Pressures. *Phys. Rev. B* **1986**, *34*, 5082.
8. Mailhiot, C.; Yang, L. H.; McMahan, M. K. Polymeric Nitrogen. *Phys. Rev. B* **1992**, *46*, 14419.
9. Radousky, H. B.; Nellis, W. J.; Ross, M.; Hamilton, D. C.; Mitchell, A. C. Molecular Dissociation and Shock-Induced Cooling in Fluid Nitrogen at High Densities and Temperatures. *Phys. Rev. Lett.* **1986**, *57*, 2419.
10. Schiferl, D.; Buchsbaum, S.; Mills, R. L. Phase Transitions in Nitrogen Observed by Raman Spectroscopy From 0.4 to 27.4 GPa at 15K. *J. Phys. Chem.* **1985**, *89*, 2324.
11. Reichlin, R.; Schiferl, D.; Martin, S.; Vanderborgh, C.; Mills, R. L. Optical Studies of Nitrogen to 130 GPa. *Phys. Rev. Lett.* **1985**, *55*, 1464.
12. Olijnyk, H.; Jephcoat, A. P. Vibrational Dynamics of Isotopically Dilute Nitrogen to 104 GPa. *Phys. Rev. Lett.* **1999**, *83*, 332.
13. Young, D. A.; Zha, C.-S.; Boehler, R.; Yen, J.; Nicol, M.; Zinn, A. S.; Schiferl, D.; Kinkead, S.; Hanson, R. C.; Pinnick, D. A. Diatomic Melting Curves to Very High Pressure. *Phys. Rev. B* **1987**, *35*, 5353.
14. Manzhelii, V. G., Freiman, Y. A., Eds. *Physics of Cryocrystals*; American Institute of Physics: Woodbury, NY, 1997.

15. Lesar, R.; Ekberg, S.; Jones, L.; Mills, R.; Schwalbe, L.; Schiferl, D. Raman Spectroscopy of Solid Nitrogen up to 374 Kbar. *Solid State Commun.* **1979**, *32*, 131.
16. Scheerboom, M.; Schouten, J. Anomalous Behavior of the Vibrational Spectrum of the High-Pressure δ Phase of Nitrogen: A Second-Order Transition. *Phys. Rev. Lett.* **1993**, *71*, 2252.
17. Eters, R.; Chandrasekharan, V.; Uzan, E.; Kobashi, K. High-Pressure Static and Dynamic Properties of the R3-C Phase of Solid Nitrogen. *Phys. Rev. B* **1986**, *33*, 8615.
18. Belek, J.; Lesar, R.; Eters, R. Calculated Thermodynamic Properties and Phase Transitions of Solid N₂ at Temperatures $0 \leq T \leq 300$ K and Pressures $0 \leq P \leq 100$ GPa. *J. Chem. Phys.* **1990**, *92*, 5430.
19. Gregoryanz, E.; Goncharov, A. F.; Sanloup, C.; Somayazulu, M.; Mao, H.-K.; Hemley, R. J. High P-T Transformations of Nitrogen to 170 GPa. *J. Chem. Phys.* **2007**, *126*, 184505.
20. Bini, R.; Ulivi, L.; Kreutz, J.; Jodl, H. J. High-Pressure Phases of Solid Nitrogen by Raman and Infrared Spectroscopy. *J. Chem. Phys.* **2000**, *112*, 8522.
21. Eremets, M. I.; Gavriluk, A. G.; Trojan, I. A.; Dzivenko, D. A.; Boehler, R. Single-Bonded Cubic Form of Nitrogen. *Nature Materials* **2004**, *3*, 558.
22. Eremets, M. I.; Gavriluk, A. G.; Trojan, I. A. Single-Crystalline Polymeric Nitrogen. *Appl. Phys. Lett.* **2007**, *90*, 171904.
23. Goncharov, A. F.; Gregoryanz, E.; Mao, H.-K.; Liu, Z.; Hemley R. J. Optical Evidence for a Nonmolecular Phase of Nitrogen Above 150 GPa. *Phys. Rev. Lett.* **2000**, *85*, 1262.
24. Gregoryanz, E.; Goncharov, A. F.; Hemley, R. J.; Mao, H.-K.; Somayazulu, M.; Shen, G. Raman, Infrared, and X-ray Evidence for New Phases of Nitrogen at High Pressures and Temperatures. *Phys. Rev. B* **2002**, *66*, 224108.
25. Mattson, W. D.; Sanchez-Portal, D.; Chiesa, S.; Martin, R. M. Prediction of New Phases of Nitrogen at High Pressure from First-Principle Simulations. *Phys. Rev. Lett.* **2004**, *93*, 125501.
26. Mattson, W. D. The Complex Nature of Nitrogen Under Pressure: Ab Initio Simulation of the Properties of Structures and Shock Waves. Ph.D. Thesis, University of Illinois at Urbana-Champaign, Champaign, IL, 2003.
27. Vos, W. L.; Finger, L. W.; Hemley, R. J.; Hu, J.-Z.; Mao, H.-K.; Schouten, J. A. A High-Pressure Van Der Waals Compound in Solid Nitrogen-Helium Mixtures. *Nature (London)* **1992**, *358*, 46.

28. Loubeyre, P.; Jean-Louis, M.; LeToullec, R.; Charon Gerard, L. High-Pressure Measurements of the He-Ne Binary Phase Diagram at 296K: Evidence for the Stability of a Stoichiometric Ne(He)₂ Solid. *Phys. Rev. Lett.* **1993**, *70*, 178.
29. Somayazulu, M. S.; Finger, L. W.; Hemley, R. J.; Mao, H.-K. High-Pressure Compounds in Methane-Hydrogen Mixtures. *Science* **1996**, *271*, 1400.
30. Loubeyre, P.; Le Toullec, R.; Pinceaux, J. P. Compression of Ar(H₂)₂ Up to 175 GPa: A New Path for the Dissociation of Molecular Hydrogen? *Phys. Rev. Lett.* **1994**, *72*, 1360.
31. Mao, H. K.; Xu, J.; Bell, P. M. Calibration of the Ruby Pressure Gauge to 800 Kbar Under Quasihydrostatic Conditions. *J. Geophys. Res.* **1986**, *91*, 4673.
32. Jayaraman, A. Diamond Anvil Cell and High-Pressure Physical Investigations. *Rev. Mod. Phys.* **1983**, *55*, 65.
33. Adar, F. Evolution and Revolution of Raman Instrumentation—Application of Available Technologies to Spectroscopy and Microscopy. In *Handbook of Raman Spectroscopy: From the Research Laboratory to the Process Line*; Lewis, I. R.; Edwards, H. G. M., Eds.; Marcel Dekker, Inc.: New York, 2001; pp 11–41.
34. Liu, Z.; Yang, H.; Hu, J.; Mao, H. K.; Hemley, R. J. High-Pressure Synchrotron X-ray Diffraction and Infrared Microspectroscopy Applications of Dense Hydrus Phases. *J. Phys. Condens. Matter* **2002**, *14*, 10641.
35. High Pressure Collaborative Access Team. <http://www.hpcat.aps.anl.gov/> (accessed October 2007).
36. Dera, P. Advanced Photon Source, Argonne National Laboratory, Argonne, IL. Private communication on the Reciprocal Space Viewer Version 1.0, October 2007.
37. Sharma, S. K.; Mao, H. K.; Bell, P. M. Raman Measurements of Hydrogen in the Pressure Range 0.2–630 Kbar at Room Temperature. *Phys. Rev. Lett.* **1980**, *44*, 886.
38. Schneider, H.; Hafner, W.; Wokaun, A.; Olijnyk, H. Room Temperature Raman Scattering Studies of External and Internal Modes of Solid Nitrogen at Pressures $8 \leq P \leq 54$ GPa. *J. Chem. Phys.* **1992**, *96*, 8046.
39. Ulivi, L.; Bini, R.; Loubeyre, P.; LeToullec, R.; Jodl, H. J. Spectroscopic Studies of the Ar(H₂)₂ Compound Crystal at High Pressure and Low Temperatures. *Phys. Rev. B* **1999**, *60*, 6502.
40. Lipp, M. J.; Klepeis, J. P.; Baer, B. J.; Cynn, H.; Evans, W. J.; Iota, V.; Yoo, C.-S. Transformation of Molecular Nitrogen to Nonmolecular Phases At Megabar Pressures. *Phys. Rev. B* **2007**, *76*, 014113.

41. Kume, T.; Sasaki, S.; Shimizu, H. Raman Study of Solid Ammonia at High Pressures and Low Temperatures. *J. Raman Spectrosc.* **2001**, *32*, 383.
42. Moulton, N. E.; Watson, G. H.; Daniels, W. B.; Brown, D. M. Raman Scattering from Fluid Hydrogen to 2500 Amagats. *Phys. Rev. A* **1988**, *37*, 2475.
43. Gregoryanz, E.; Goncharov, A. F.; Hemley, R. J.; Mao, H.-K. High-Pressure Amorphous Nitrogen. *Phys. Rev. B* **2001**, *64*, 052103.
44. Mao, H.-K.; Hemley, R. J. Optical Transitions in Diamond at Ultrahigh Pressures. *Nature (London)* **1991**, *351*, 721.
45. Tassini, L.; Gorelli, F.; Ulivi, L. High Temperature Structures and Orientational Disorder in Compressed Solid Nitrogen. *J. Chem. Phys.* **2005**, *122*, 074701.
46. Iota, V.; Yoo, C. S. Phase Diagram of Carbon Dioxide: Evidence for a New Associated Phase. *Phys. Rev. Lett.* **2001**, *86*, 5922.

NO. OF
COPIES ORGANIZATION

1 DEFENSE TECHNICAL
(PDF INFORMATION CTR
only) DTIC OCA
8725 JOHN J KINGMAN RD
STE 0944
FORT BELVOIR VA 22060-6218

1 US ARMY RSRCH DEV &
ENGRG CMD
SYSTEMS OF SYSTEMS
INTEGRATION
AMSRD SS T
6000 6TH ST STE 100
FORT BELVOIR VA 22060-5608

1 DIRECTOR
US ARMY RESEARCH LAB
IMNE ALC IMS
2800 POWDER MILL RD
ADELPHI MD 20783-1197

1 DIRECTOR
US ARMY RESEARCH LAB
AMSRD ARL CI OK TL
2800 POWDER MILL RD
ADELPHI MD 20783-1197

1 DIRECTOR
US ARMY RESEARCH LAB
AMSRD ARL CI OK T
2800 POWDER MILL RD
ADELPHI MD 20783-1197

ABERDEEN PROVING GROUND

1 DIR USARL
AMSRD ARL CI OK TP (BLDG 4600)

NO. OF
COPIES ORGANIZATION

ABERDEEN PROVING GROUND

3 DIR USARL
AMSRD ARL WM BD
J CIEZAK